J. Mech. Phys. Solids 176 (2023) 105300

Contents lists available at ScienceDirect

Journal of the Mechanics and Physics of Solids

journal homepage: www.elsevier.com/locate/jmps

Dislocation climb driven by lattice diffusion and core diffusion

Fengxian Liu [a,c,*], Alan C.F. Cocks [b], Edmund Tarleton [b,a]

[a] Department of Materials, University of Oxford, Parks Road, Oxford OX1 3PH, UK
[b] Department of Engineering Science, University of Oxford, Parks Road, Oxford OX1 3PJ, UK
[c] Department of Mechanics of Solids, Surfaces and Systems, Faculty of Engineering Technology, University of Twente, Drienerlolaan 5, 7522NB Enschede, The Netherlands

ARTICLE INFO

Keywords:
Core diffusion
Lattice diffusion
Dislocation dynamics
Variational principle

ABSTRACT

Diffusion of material has a crucial influence on dislocation motion, particularly at elevated temperatures. It is generally believed that, in a single crystal, lattice diffusion prevails when the temperature is high and core diffusion dominates at relatively low temperatures. Due to the complexity of modeling the coupling between core and lattice diffusion, a given physical problem is often simplified into two extremes where only one of the two diffusion regimes is considered. However, a quantitative definition of the conditions under which each of the diffusion mechanisms is dominant is still lacking. In the present work, we employ a variational principle for the analysis of microstructure evolution; we demonstrated how finite element (FE) based analysis can be developed from it, in which the competition and synergy between core diffusion and lattice diffusion can be naturally taken into consideration. A dislocation climb model is further developed by incorporating the FE analysis into the nodal based three-dimensional dislocation dynamics framework, which also considers glide and cross-slip processes.

A systematic study of the coalescence of prismatic dislocation loops (PDLs) at various conditions is conducted based on the proposed method; together with the analytical solutions of the motion of a circular PDL controlled by core and lattice diffusion, a diffusion mechanism map is constructed, which provides useful guidance on determining the dominant diffusion mechanism for given loop sizes, spacing, and temperature. The results show that, in a practical loop coarsening process, core diffusion provides a fast short circuit for local atomic rearrangement, so that it is dominant when loop size or the distance between loops is small, particularly at temperatures lower than $0.5T_m$ (T_m is the melting point of a given material). While, at high temperatures, when the distance between loops is large or when the loop size is large, lattice diffusion becomes more efficient. The present findings indicate that simultaneous consideration of both core and lattice diffusion is necessary to quantitatively understand the microstructure evolution for dislocation climb related physical processes, such as creep and post-irradiation annealing.

1. Introduction

At elevated temperatures, many physical processes which occur in a crystalline material require the diffusion of matter, either by lattice, dislocation core, grain boundary, or surface diffusion (Shewmon, 2016). Here we are interested in how diffusion can aid the motion of dislocations. We assume that dislocations are perfect sources and sinks for vacancies. The addition of atoms or vacancies

* Corresponding author at: Department of Materials, University of Oxford, Parks Road, Oxford OX1 3PH, UK.
E-mail address: fengxian.liu@materials.ox.ac.uk (F. Liu).

https://doi.org/10.1016/j.jmps.2023.105300
Received 7 December 2022; Received in revised form 23 March 2023; Accepted 12 April 2023
Available online 25 April 2023

to the core of an edge dislocation allows it to climb. This can be accomplished through two mechanisms: core diffusion and lattice diffusion. Core diffusion, also known as pipe diffusion, refers to the transportation of atoms or vacancies along the core of the dislocation; while lattice diffusion, also known as bulk diffusion, involves the transfer of atoms or vacancies from the surrounding lattice to the dislocation lines. Both processes contribute to climb of the dislocation. The solid state diffusion of matter is driven by the gradient of the chemical potential of the diffusing species. The main contributions to this gradient are from the gradient of stress acting normal to the dislocation line in the case of core diffusion and by the gradient of concentration of point defects in the case of lattice diffusion. Under many practical circumstances, the two diffusion processes are coupled in promoting dislocation climb motion. Because of the complex dislocation networks involved, analytical solutions of governing equations for this coupled problem are difficult to obtain. As these two diffusion processes occur simultaneously, the faster will govern the climb process during dislocation evolution. A given physical problem is often simplified into two extreme situations: (a) the core diffusion limit; (b) the lattice diffusion limit.

At the extreme of core diffusion, it is assumed that lattice diffusion is negligible in the time window of interest, and matter is transported only along the dislocation core region. The highly disordered dislocation core lowers the activation energy for diffusion, leading to a much higher diffusivity for core diffusion. As a result, dislocations can climb at a faster rate, and matter cannot be exchanged between different dislocations unless they intersect. Therefore, the resulting dislocation climb motion is referred to as self-climb, or conservative climb. In self-climb, atoms are rapidly rearranged in the core region to balance the difference of chemical potential along the dislocation line. Rapid core diffusion is observed to play a decisive role in a wide variety of material behaviors involving dislocations, impurities and precipitates, e.g., creep (Love, 1964), dynamic strain aging (Schwink and Nortmann, 1997), facilitating Ostwald ripening of a new phase (Vengrenovich et al., 2002), phase separation (Nicolas et al., 2020) and device failure (Garbrecht et al., 2017), or accelerating the diffusion of impurities (Legros et al., 2008) in thin films. The governing equations for this one-dimensional diffusion along the dislocation line can be obtained from the variational principle of microstructural evolution (Liu et al., 2020b,a), following the pioneering work of Needleman and Rice (1983) and Cocks et al. (1998). These equations have been implemented into a nodal based three-dimensional dislocation dynamics (3D-DDD) framework to investigate the fast loop coarsening during post-irradiation annealing (Liu et al., 2020b) and the particle bypass mechanisms (Liu et al., 2021) during low temperature creep.

At the extreme of lattice diffusion, more attention is paid to the mass exchange between the core of the climbing dislocation and the boundary of the crystal. Dislocation cores only serve as either a source or sink for matter and provide a boundary condition for the chemical potential, linking the forces acting on the dislocations to the potential at the boundaries of the cores. Gao and Cocks (2009) obtained the governing equations for lattice diffusion by a thermodynamic variational approach, similar to Eq. (2.16)-Eq. (2.18), as derived below. However, solving this set of governing equations, subject to the condition that the chemical potential is in equilibrium near each dislocation core as well as external boundary conditions appropriate for the domain, is complex and time-consuming. The difficulty lies in tracking the internal boundaries of dislocation cores continuously during fast dislocation evolution. Earlier attempts began with developing analytical climb models, based on dislocation dynamics (DD) methods, using the equilibrium solution in a prescribed uniform vacancy field (Mordehai et al., 2008; Bakó et al., 2011; Davoudi et al., 2012; Liu et al., 2017a). These models have provided useful results for climb-enabled dislocation plasticity but they can only be applied to situations where analytical solutions for bulk diffusion are available, such as a single straight dislocation or a prismatic dislocation loop (PDL). For more general situations, analytical solutions are usually too difficult to obtain and numerical methods are often adopted. Ayas et al. (2014) and Keralavarma and Benzerga (2015) developed a methodology for diffusion mediated dislocation climb where a superposition method proposed by Van der Giessen and Needleman (1995) is used to obtain the dislocation mechanical fields and solve the vacancy diffusion equations on the same finite element grid. The core-level boundary conditions for the vacancy concentration field are avoided by invoking a suitable approximation. The superposition method provides a practical method for looking at the collective dislocation behavior at high temperatures, such as creep. Application of this method is limited to two-dimensional simulations where dislocation lines are simplified as points so that they can be easily treated as sources/sinks for the diffusing species. Following this approach, Liu et al. (2017b) proposed a discrete–continuum method in three dimensions, where the continuum concentration fields around dislocation cores are localized to the discrete FE nodes by a distance-related weight function. This method has proved to be effective in modeling high-temperature annealing of micropillars, but the computational efficiency is still limited by the localization method when the dislocation network is complicated. More recently, Gu et al. (2015) circumvented the computational complexity by incorporating a Green's function formulation of dislocation climb into a 3D DD model, providing an ideal non-local approach for the long-range effect of vacancy diffusion. Po and Ghoniem (2014) proposed a variational formulation of dislocation motion constrained by the diffusion of point defects, which was numerically implemented into DD to simulate dislocation motion confined to channels and pillars.

For more general situations, core diffusion and lattice diffusion occur simultaneously and couple with each other in assisting the climb of dislocations. Only a few attempts have been made to couple core and lattice diffusion in a dislocation climb model. Geslin et al. (2015) proposed a phase-field model to analyze the climb of an isolated, straight edge dislocation by solving both the core diffusion and lattice diffusion equations. Niu et al. (2017) developed a dislocation climb model based on a stochastic scheme at the atomistic scale, which considers both vacancy lattice diffusion and core diffusion to model the stochastic motion of jogs and the hop of vacancies at each discrete lattice site. This approach was later implemented by Gu et al. (2018) to analyze dislocation climb during self-healing of low-angle grain boundaries. However, the complexity involved in these models makes large scale simulations out of reach. It is evident that a given change in the dislocation network, e.g. the size or shape change of a PDL, can result from different kinetic processes, including core diffusion controlled self-climb (conservative climb) and lattice diffusion controlled non-conservative climb. It is therefore important to identify the appropriate kinetic process and to determine under what condition,

e.g. the temperature and stress level, a given mechanism dominates. A systematic, quantitative interpretation is still lacking in the literature. Only recently, the dynamics of dislocations during loop annealing involving both core diffusion controlled self-climb and lattice diffusion controlled vacancy-mediated climb have been investigated by Breidi and Dudarev (2022), in which the climb velocity contributed from bulk diffusion is derived from the analytical solution of a radial flux pattern as used by Mordehai et al. (2009). To solve the coupled diffusion problem, two challenges need to be addressed: (a) an efficient method to solve the lattice diffusion part of the problem for any arbitrary dislocation networks and (b) satisfying the continuity conditions at the interface between bulk and core regions. We have developed a self-climb model based on a finite element type of numerical technique that can solve core diffusion equations for any arbitrary dislocation network within a nodal based DD framework (Liu et al., 2020b,a). A natural extension of this technique is to combine it with the finite element analysis for the lattice diffusion part of the problem so that the coupled diffusion equations can be solved in a unified framework.

Here we start from a general strategy for modeling microstructural evolution which can be adapted to deal with both core and lattice diffusion. The approach is based on a variational principle that is applicable when considering the competition between all possible dissipative processes that are driven by a number of thermodynamic driving forces. The general variational principle based approach, developed by Cocks (1996), Cocks et al. (1998), is a global work rate minimization technique and has been proved to be efficient in studying a series of mass transport mechanisms, including grain-boundary diffusion (Cocks, 1989; Needleman and Rice, 1983; Pan and Cocks, 1995), interface/surface diffusion (Cocks, 1992; Pan et al., 1997; Suo, 1997), grain-boundary migration (Gill and Cocks, 1996) and coupled grain-boundary and surface diffusion (Pan et al., 1997). Basic kinetic equations for lattice diffusion and core diffusion are derived first in Section 2. In Section 3, we show how the numerical scheme is developed from the variational principle to model the lattice diffusion and the resulting climb motion. A typical example is given to validate the proposed numerical method in Section 4. The core and lattice diffusion processes are then coupled, in Section 5, in a unified DD framework to give a straightforward picture of the dominant diffusion regime.

2. Methodology

In this section, we develop the governing equations for lattice diffusion and core diffusion, respectively, based on a variational principle, which has been rigorously formulated for a series of mass transport mechanisms. The variational functional of a given system Π is defined as,

$$\Pi = \Psi + \dot{G} \tag{2.1}$$

where Ψ is a rate potential term involving contributions from all possible dissipative processes. $\dot{G}$ is the energy rate term, which is the origin of the generalized thermodynamic force. An attractive feature of this approach is that a wide range of different kinetic processes and driving forces can readily be incorporated into the formalism. It is the combination of thermodynamics and kinetics that determines the actual evolution path and the final state. The essential idea carries over to core and lattice diffusion. That is, *among all the virtual velocities that describe the rate of evolving microstructure and virtual diffusive fluxes that satisfy mass conservation, the actual velocity and flux fields minimize the functional of the system Π* (Pan et al., 1997). Consider the general situation of a coupled diffusion problem as schematically shown in Fig. 1. A body of volume V and surface S is subjected to surface traction T_s. For convenience, we cut the core regions from the body along the cylindrical boundary of the dislocation core Γ and treat the bulk and core volume independently. In the bulk, a body of volume V^*, with an external surface S and internal surfaces Γ, is considered. The transport of matter in the bulk occurs through lattice diffusion. However, in the core, diffusion is assumed to be extremely fast across the core, resulting in a constant chemical potential at a specific sectional area, varying only along the direction of the dislocation line. Therefore, consideration is only given to mass diffusion along the dislocation line through core diffusion. We now proceed to determine the contributions to the functional Π, in Eq. (2.1), for the bulk region and core region, respectively. The problem considered here falls into an important class of problems in which the two diffusion paths are completely independent of each other, but diffusion along these paths is subjected to a combined set of boundary conditions at the surface and dislocation cores. For this class of problem, we can write Eq. (2.1) in the form

$$\Pi(\dot{a}_i, \dot{b}_i) = \Psi(\dot{a}_i, \dot{b}_i) + \dot{G}(\dot{a}_i, \dot{b}_i) = \Psi(\dot{a}_i) + \dot{G}(\dot{a}_i) + \Psi(\dot{b}_i) + \dot{G}(\dot{b}_i) \tag{2.2}$$

where $\dot{a}_i$ and $\dot{b}_i$ are rate quantities associated with each of the diffusion paths (core and lattice diffusion for the current problem of interest). Minimizing the function then gives two uncoupled sets of rate equations to solve

$$\left(\frac{\partial \Psi(\dot{a}_i)}{\partial \dot{a}_i} + \frac{\partial \dot{G}(\dot{a}_i)}{\partial \dot{a}_i}\right) \delta \dot{a}_i = 0 \tag{2.3}$$

$$\left(\frac{\partial \Psi(\dot{b}_i)}{\partial \dot{b}_i} + \frac{\partial \dot{G}(\dot{b}_i)}{\partial \dot{b}_i}\right) \delta \dot{b}_i = 0 \tag{2.4}$$

Thus, for a given configuration, the rates of the two processes can be determined independently of each other. The coupling occurs through a combination of the rates, which determines how the microstructure evolves. We illustrate this later by studying a series of simple problems, but first, we evaluate the evolution process for lattice and core diffusion within the context of Eqs. (2.3) and (2.4).

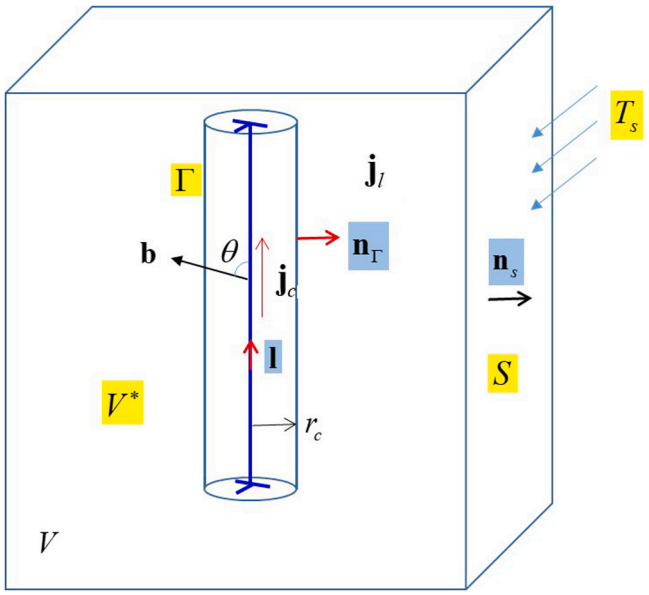

Fig. 1. Schematic of domains for lattice diffusion and core diffusion.

2.1. Lattice diffusion

The constitutive behavior of all the diffusional processes, including lattice, core, grain boundary, and surface diffusion, can be represented in the same general form. The diffusive flux, $\boldsymbol{j}$, defined as the volume of mass flowing across a unit area perpendicular to the flux direction per unit time, is linearly dependent on the gradient of the chemical potential of the diffusing species,

$$\boldsymbol{j} = -D\frac{\partial \mu}{\partial \boldsymbol{s}} \tag{2.5}$$

where μ is the chemical potential, D is the effective diffusivity and $\boldsymbol{s}$ is a local coordinate along the diffusion path.

For lattice diffusion, we consider the flux of atoms across a unit area within a body, $\boldsymbol{j}_l$, so that

$$\boldsymbol{j}_l = -D_l \nabla \mu = D_l \boldsymbol{f} \tag{2.6}$$

where the subscription 'l' is used to describe lattice diffusion related variables, and subscription 'c' represents core diffusion. ∇ is the gradient vector operator. $D_l = D_{lattice}\Omega/kT$ is the effective lattice diffusivity, where $D_{lattice}$ denotes the lattice diffusion coefficient, Ω indicates atomic volume, k is Boltzmann's constant, and T is the absolute temperature. The flux is driven by the potential gradient $\nabla\mu$, so that $\boldsymbol{f} = -\nabla\mu$ is a driving force. During the diffusion process, energy is dissipated. Cocks et al. (1998) demonstrated that the dissipation rate potential can be expressed in terms of the diffusion flux,

$$\psi_l = \frac{1}{2D_l}\boldsymbol{j}_l \cdot \boldsymbol{j}_l, \quad \text{such that} \quad f = \frac{\partial \psi_l}{\partial j_l} \tag{2.7}$$

The total rate potential in the bulk region is then given by,

$$\Psi_l = \int_{V^*} \psi_l dV = \int_{V^*} \frac{1}{2D_l}\boldsymbol{j}_l \cdot \boldsymbol{j}_l dV \tag{2.8}$$

We assume that dislocations serve as idea sources or sinks for the diffusing species, such that all the work done during the diffusion process is available to drive the diffusive flux of matter. According to Gao and Cocks (2009), the rate change of Gibbs free energy in the bulk, with external boundary S and internal boundary Γ, is,

$$\dot{G}_l = \int_{V^*} \mu_l(-\nabla \cdot j_l)\mathrm{d}V + \int_S T_s \dot{u}_s dS + \int_L f_{cl}\dot{u}_d dl \tag{2.9}$$

where u_s and u_d are the displacements due to the plating of atoms at the external surface S and the internal dislocation core boundary Γ, L is the total length of the dislocation line, f_{cl} is the climb component of the Peach–Kohler force acting on the dislocation core.

When matter flows across the boundary, atoms must be added to or removed from the surface. If we consider an element of area dA with outward unit vector $\boldsymbol{n}_s$ on S, the total volume of atoms crossing dA in a time interval dt is $\boldsymbol{j}_l \cdot \boldsymbol{n}_s dA dt$. In this process the surface, S, moves normal to itself by an amount $du_s = -\boldsymbol{j}_l \cdot \boldsymbol{n}_s dt$, so that

$$\dot{u}_s = -\boldsymbol{j}_l \cdot \boldsymbol{n}_s \tag{2.10}$$

The negative sign '-' means that a positive atomic flux passing through the external surface S will lead to the shrinkage of the volume, resulting in a negative displacement of the surface.

Similarly, when matter flows across dislocation cores, Γ, atoms are added or removed from the dislocation core, leading to climb of the dislocation. During this process, the net volumetric flux of atoms into a unit length of dislocation is $\oint_\Gamma \boldsymbol{j}_l \cdot \boldsymbol{n}_\Gamma d\Gamma$. Mass conservation then requires that this flux of atoms is directly responsible for the climb process, i.e.,

$$\dot{u}_d = v_l \tag{2.11}$$

$$v_l b_e = -\oint_\Gamma \boldsymbol{j}_l \cdot \boldsymbol{n}_\Gamma d\Gamma \tag{2.12}$$

where b_e is the edge component of the Burgers vector and v_l is the climb rate of the dislocation caused by lattice diffusion. Eq. (2.12) indicates that when a positive atomic flux flows into the dislocation core, i.e, dislocation absorbs atoms, the inserted plane of an edge dislocation moves downwards, which results in a negative climb rate for a dislocation with a positive Burgers vector and vice versa.

With the divergence theorem, the first term on the right hand side of Eq. (2.9) can be expanded as,

$$\int_{V^*} \mu_l \cdot (-\nabla j_l) \mathrm{d}V = \int_{V^*} \nabla \mu_l \cdot \boldsymbol{j}_l \mathrm{d}V - \int_S \mu_l \boldsymbol{j}_l \cdot \boldsymbol{n}_s dS - \int_\Gamma \mu_l \boldsymbol{j}_l \cdot \boldsymbol{n}_\Gamma d\Gamma \tag{2.13}$$

Substituting Eq. (2.10), Eq. (2.11) and (2.13) into Eq. (2.9), we obtain,

$$\dot{G}_l = \int_{V^*} \nabla \mu_l \cdot \boldsymbol{j}_l \mathrm{d}V - \int_S \mu_l \boldsymbol{j}_l \cdot \boldsymbol{n}_s dS - \int_\Gamma \mu_l \boldsymbol{j}_l \cdot \boldsymbol{n}_\Gamma d\Gamma - \int_S T_s \boldsymbol{j}_l \cdot \boldsymbol{n}_s dS + \int_L f_{cl} v_l dl \tag{2.14}$$

We can now construct Π_l for the bulk, by adding Eqs. (2.8) and (2.14),

$$\Pi_l = \int_{V^*} \nabla \mu_l \cdot \boldsymbol{j}_l \mathrm{d}V - \int_S \mu_l \boldsymbol{j}_1 \cdot \boldsymbol{n}_s dS - \int_\Gamma \mu_l \boldsymbol{j}_l \cdot \boldsymbol{n}_\Gamma d\Gamma - \int_S T_s \boldsymbol{j}_l \cdot \boldsymbol{n}_s dS + \int_L f_{cl} v_l dl + \int_{V^*} \frac{1}{2D_l} \boldsymbol{j}_l \cdot \boldsymbol{j}_l dV, \tag{2.15}$$

Minimizing the functional Π_l with respect to $\mathbf{j}_l$ and v_l leads to the following governing equations for the lattice diffusion processes in the bulk region,

$$\nabla \mu_l = -\frac{\mathbf{j}_l}{D_l}, \quad \text{in } V^* \tag{2.16}$$

$$\mu_l = T_s \, \mathbf{n}_s, \quad \text{on } S \tag{2.17}$$

$$\mu_l = -f_{cl}/b, \quad \text{on } \Gamma \tag{2.18}$$

These kinetic equations, together with Eq. (2.12), govern the lattice diffusion process and the resulting climb motion. Eq. (2.17) and (2.18) ensure continuity of chemical potential at the external boundary S and on the core cylinder Γ. Solving these equations gives the flux pattern and climb velocity in the bulk area.

2.2. Core diffusion

In the core area, mass can only diffuse along the dislocation line, which also follows the classical description of diffusion. Similar to Eq. (2.16), the volumetric flux by core diffusion, j_c, is driven by the chemical potential gradient,

$$j_c = -D_c \frac{\partial \mu_c}{\partial l} \tag{2.19}$$

where $D_c = a_c D_{core} \Omega / kT$ is the effective core diffusivity, with D_{core} denoting the core diffusion coefficient and a_c is the sectional area of the dislocation core. Diffusion of matter along the dislocation core also dissipates energy. The rate potential for core diffusion is,

$$\Psi_c = \int_L \frac{1}{2D_c} \boldsymbol{j}_c \cdot \boldsymbol{j}_c dl \tag{2.20}$$

The rate of change of Gibbs free energy $\dot{G}_c$ is,

$$\dot{G}_c = \int_L f_{cl} v_c dl \tag{2.21}$$

where v_c is the climb rate resulting from the core diffusion process, and as noted earlier f_{cl} is the climb component of the Peach–Kohler force.

Summing contributions from Eqs. (2.20) and (2.21) into the functional for the core area, we construct Π_c as,

$$\Pi_c = \Psi_c + \dot{G}_c = \int_L \frac{j_c^2}{2D_c} dl + \int_L f_{cl} v_c dl \tag{2.22}$$

Minimizing the functional Π_c with respect to j_c and v_c gives,

$$\delta \Pi_c = \int_L \frac{j_c}{D_c} \delta j_c dl + \int_L f_{cl} \delta v_c dl = 0 \tag{2.23}$$

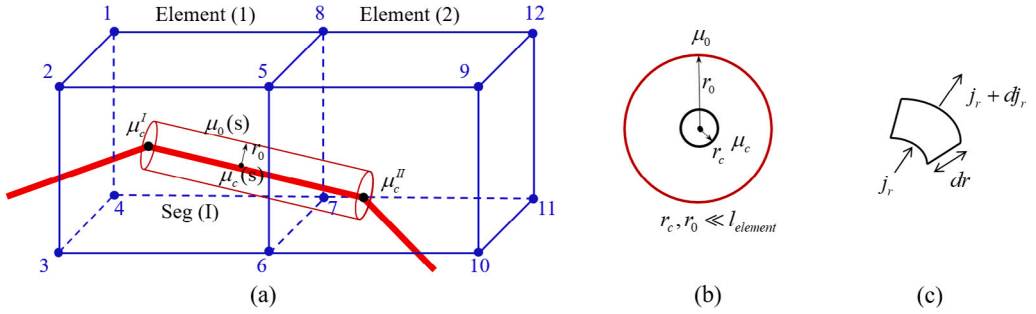

Fig. 2. Schematic of the discretization method. (a) a dislocation segment, Seg (I), passes through two finite elements, element (1) and element (2). (b) a cylindrical region centered on the dislocation core. (c) the radial flux pattern near the dislocation core.

Also, mass conservation, in the core diffusion controlled climb process, requires that the net volumetric flux of vacancies into a unit length of dislocation dl should be consumed by the climb motion, i.e.,

$$v_c b_e dl + dj_c = 0 \tag{2.24}$$

Eqs. (2.23) and (2.24) give the governing equations of core diffusion and the resulting self-climb rate.

2.3. Continuity

It proves convenient in the derivation of the variational principle for lattice diffusion, to express the response in terms of the chemical potential μ. While when considering the core diffusion process, it is generally more straightforward to express the behavior in terms of volumetric flux j. To guarantee the continuity of chemical potential on the boundary between the lattice and core diffusion, we have,

$$\mu_l = \mu_c, \quad \text{on } \Gamma \tag{2.25}$$

Note that, Eq. (2.16)–(2.12) and (2.18) give the chemical potential μ_l and the climb rate contributed from the lattice diffusion process v_l. Eqs. (2.23) and (2.24) give the flux pattern j_c and the climb rate related to the core diffusion regime v_c. Then, the climb rate resulting from the coupled lattice and core diffusion process can be derived as,

$$v_{climb} = v_l + v_c \tag{2.26}$$

3. Implementation

In this section, we describe how the variational principle presented in the previous section can be used to aid the development of numerical procedures for modeling microstructure evolution in engineering materials. We start by discretizing the lattice diffusion formulation into the nodal based 3D-DDD framework to simulate the resulting climb process. We then add the core diffusion process to examine their interaction under different conditions.

3.1. Discretization of the volume

To solve Eqs. (2.16)–(2.18), we discretize the body V, as shown in Fig. 2(a). We divide V into finite elements. Along the sides of each element, we designate nodes that define the element's shape. The full set of nodes and elements represent the body V. The number of nodes in the mesh is designated as N_n and the number of elements N_e. Here, we follow the convention that FE nodal values are numbered by a subscript, for example, μ_1 represents the nodal chemical potential at node 1, whereas FE elemental values are identified by superscript with parentheses, for example, $\mu^{(1)}$ is the chemical potential of element (1).

We wish to obtain the unknown chemical potential field, $\mu(\mathbf{X})$, within the domain V. Consider a finite element (1) with FE nodes $1, 2, \ldots, 8$, as shown in Fig. 2(a). We define the chemical potential within the element using shape functions as follows,

$$\mu^{(1)}(\mathbf{X}) = \left[N_e^{(1)}(\mathbf{X})\right]\left[\mu_e^{(1)}\right] \tag{3.1}$$

where $\mathbf{X}$ is the location in the domain, $[\mu_e^{(1)}] = [\mu_1 \ \ \mu_2 \ \ \ldots \ \ \mu_8]^T$ is the discrete (unknown) nodal chemical potential matrix of the FE elements, $[N_e^{(1)}(\mathbf{X})] = [N_1^{(1)} \ \ N_2^{(1)} \ \ \ldots \ \ N_8^{(1)}]$ is the (known) shape function matrix of element (1), which we will discuss further later. Then, we derive the flux $\mathbf{j}$ according to Eq. (2.16),

$$\mathbf{j}^{(1)}(\mathbf{X}) = -D_l \nabla \mu^{(1)}(\mathbf{X}) = -D_l \left[B^{(1)}\right]\left[\mu_e^{(1)}\right] \tag{3.2}$$

where $[B^{(1)}] = \left[\frac{\partial N_e^{(1)}(\mathbf{X})}{\partial X}\right]$.

Similarly, we treat the dislocation as a line that moves through the body and divide the dislocation lines into a series of line elements with effective nodal forces specified at the nodes. Variables associated with dislocation segments/nodes on the core boundary are also denoted with a subscript c to distinguish them from the FE elements/nodes. Consider a straight dislocation segment (I) bounded by dislocation nodes I and II, as shown in Fig. 2(a). A local coordinate s is defined. The origin of s is located at the mid-point of the segment and the positive direction points from node $I \rightarrow II$. s is normalized by half of the segment length $l_{(I)}/2$, so that $s = -1$ at node I, $s = 1$ at node II. We define the chemical potential along segment (I) by the shape functions,

$$\mu_c^{(I)}(s) = \left[N_c^{(I)}(s)\right]\left[\mu_c^{(I)}\right] \tag{3.3}$$

where $s \in [-1, 1]$, $\left[\mu_c^{(I)}\right] = \begin{bmatrix} \mu_{cI} & \mu_{cII} \end{bmatrix}^T$ is the discrete (known) nodal chemical potential matrix within the dislocation core, $[N_c(s)] = \begin{bmatrix} N_{cI}(s) & N_{cII}(s) \end{bmatrix}$ is the (known) shape function matrix. Assuming a linear variation of climb velocity along each segment,

$$v_l^{(I)}(s) = \left[N_c^{(I)}(s)\right]\left[v_l^{(I)}\right] \tag{3.4}$$

where $[v_l^{(I)}] = [v_I \quad v_{II}]$ is the elemental matrix of nodal climb velocities of segment (I) caused by lattice diffusion.

3.2. Variational statement

For steady state lattice diffusion,

$$\nabla \cdot \mathbf{j} = \mathbf{0}, \quad \text{in} V \tag{3.5}$$

so that,

$$\omega \nabla \cdot \mathbf{j} = \mathbf{0}, \quad \text{in} V \tag{3.6}$$

where ω is an arbitrary parameter. Using the divergent theorem and substituting Eq. (2.16) into Eq. (3.6),

$$\int_V \omega \nabla \cdot \mathbf{j} dV = \int_V \nabla\omega \cdot (D_l \nabla\mu) dV + \int_S \omega \mathbf{j} \cdot \mathbf{n}_S dS + \int_\Gamma \omega \mathbf{j} \cdot \mathbf{n}_\Gamma dl = 0 \tag{3.7}$$

Since $\mu = [N][\mu_N]$ and assuming $\omega = [N][\omega_N]$,

$$\nabla\mu = [B][\mu_N] \tag{3.8}$$

$$\nabla\omega = [B][\omega_N] \tag{3.9}$$

Then Eq. (3.7) becomes,

$$[w_N]^T \left(\int_V [B]^T D_l [B] dV [\mu_N] + \int_S [N]^T \mathbf{j} \cdot \mathbf{n}_S dS + \int_\Gamma [N_c]^T \mathbf{j} \cdot \mathbf{n}_\Gamma dl \right) = 0 \tag{3.10}$$

Since $[\omega_N]^T$ is arbitrary, the term in () must be 0. For a closed system, mass is conserved in the volume, so that the second term in the () is 0. Then Eq. (3.10) can be rewritten as,

$$\int_V [B]^T D_l [B] dV [\mu_N] + \int_\Gamma [N_c]^T \mathbf{j} \cdot \mathbf{n}_\Gamma dl = 0 \tag{3.11}$$

Note, from the relationship between the flux j for lattice diffusion and the resulting climb velocity v_l, as demonstrated in Eq. (2.12), we have

$$-\oint_\Gamma \mathbf{j} \cdot \mathbf{n}_\Gamma ds = \int_L v_l(s) b_e(s) ds \tag{3.12}$$

where L is the total length of dislocation within the domain. $v_l(s)$ is the climb velocity caused by lattice diffusion. $b_e(s)$ is the edge component of the Burgers vector.

By substituting Eq. (3.4) into Eq. (3.12), we can rewrite the second term on the right hand side of Eq. (3.11) as,

$$\int_\Gamma [N_c]^T \mathbf{j} \cdot \mathbf{n}_\Gamma ds = -\left(\int_L [N_c]^T [N_c] b_e ds \right) [v_l] \tag{3.13}$$

Substituting Eq. (3.13) into Eq. (3.11), Eq. (3.11) can be rewritten as,

$$[K][\mu_N] - [K_{vc}][v_l] = 0 \tag{3.14}$$

With,

$$[K] = \int_V [B]^T D_l [B] dV \tag{3.15}$$

$$[K_{vc}] = \int_L [N_c]^T [N_c] b_e ds \tag{3.16}$$

where $[K]$ is the global viscosity matrix for lattice diffusion, $[K_{vc}]$ is a constraint matrix which relates the diffusive flux j to the climb velocity through mass conservation. Note that, within Eq. (3.14), both the nodal chemical potential of the FE elements $[\mu_N]$ and the nodal climb velocity of the dislocation segments $[v_l]$ are unknown. What we know in this system is the nodal chemical potential at the dislocation core according to Eq. (2.18). We now leverage the known chemical potential at the dislocation core to solve Eq. (3.14) with the following near core approximation.

3.3. Finite elements near dislocation core

To solve Eq. (3.14), we, therefore, need to transform the known chemical potential at the dislocation core to the FE nodes. To achieve this, we assume a cylindrical transitional region around the dislocation core with a radial flux pattern, as the cylinder shown in Fig. 2(a). We treat the dislocation as a line that moves through a body in which the element size of the mesh used to model diffusion is much larger than the core radius r_c, as shown in Fig. 2. The chemical potential μ is assumed to be distributed within a cylindrical region with a radius r_0 centered on the core in a manner that aligns with a radial flux pattern, as depicted in Fig. 2(b). μ_0 is the chemical potential on the surface of the diffusion cylinder. Note that r_0 and r_c are both much smaller than the FE element size, i.e, $r_c, r_0 \ll l_{element}$. Here, we do not have to discretize this cylindrical region around the core — we view the dislocation as a line element and r_0 and r_c are parameters we select within the implementation of the methodology.

For a radial flux pattern, as shown in Fig. 2(c), mass conservation requires that,

$$(j_r + dj_r)(r + dr)d\theta - j_r r d\theta = 0 \tag{3.17}$$

where j_r is the diffusive flux at position r. so that,

$$j_r = \frac{A}{r} \tag{3.18}$$

where A is a constant, determined by the boundary conditions.

We can either write Fick's law in terms of concentration or chemical potential, the resulting structure is the same. Here we write j_r in terms of chemical potential to keep consistent with the above description,

$$j_r = -D_l \frac{\partial \mu}{\partial r} \tag{3.19}$$

Consider boundary conditions, such that,

$$\mu = \mu_c, \quad at \quad r = r_c \tag{3.20}$$

$$\mu = \mu_0, \quad at \quad r = r_0 \tag{3.21}$$

Substituting Eq. (3.18) into Eq. (3.19), with the boundary conditions in Eqs. (3.20) and (3.21), we can derive the expressions for the flux j_r and chemical potential μ,

$$A = -\frac{D_l(\mu_0 - \mu_c)}{\ln(r_0/r_c)} \tag{3.22}$$

$$\mu = \mu_c + (\mu_0 - \mu_c)\frac{\ln(r/rc)}{\ln(r_0/r_c)} \tag{3.23}$$

$$j_r = \frac{A}{r} = -\frac{D_l(\mu_0 - \mu_c)}{r\ln(r_0/r_c)} \tag{3.24}$$

Therefore, within the near core region, i.e, within the cylinder shown in Fig. 2(a), the chemical potential is,

$$\mu(s) = \mu_c(s) + \left[\mu_0(s) - \mu_c(s)\right]\frac{\ln(r/rc)}{\ln(r_0/r_c)} \tag{3.25}$$

For a cylindrical region of length ds centered on the core, from Eq. (3.25),

$$\frac{d\mu(s)}{dr} = \frac{1}{r\ln(r_0/r_c)}[1 \quad -1]\begin{bmatrix}\mu_0(s)\\ \mu_c(s)\end{bmatrix} = [B]\begin{bmatrix}\mu_0(s)\\ \mu_c(s)\end{bmatrix} \tag{3.26}$$

with $[B] = \frac{1}{\ln(r_0/r_c)}\left[1/r \quad -1/r\right]$.

Consider $r_0, r_c \ll l_{element}$, with Eqs. (3.1) and (3.3), $\mu_0(s)$ can be interpolated from the nodal chemical potential of the FE nodes $[\mu_e]$ and $\mu_c(s)$ can be interpolated from the chemical potential of the dislocation nodes $[\mu_c]$. So that,

$$[\mu_N] = \begin{bmatrix}\mu_0(s)\\ \mu_c(s)\end{bmatrix} = [C]\begin{bmatrix}[\mu_e]\\ [\mu_c]\end{bmatrix} \tag{3.27}$$

with

$$[C] = \begin{bmatrix}[N_e(s)] & [0]\\ [0] & [N_c(s)]\end{bmatrix} \tag{3.28}$$

Eq. (3.26) can then be rewritten as,

$$\frac{d\mu(s)}{dr} = [B][\mu_N] = [B][C]\begin{bmatrix}[\mu_e]\\ [\mu_c]\end{bmatrix} \tag{3.29}$$

So that the first term on the right hand side of Eq. (3.14) is,

$$[K][\mu_N] = [K']\begin{bmatrix} [\mu_e] \\ [\mu_c] \end{bmatrix} \tag{3.30}$$

with

$$[K'] = \int_V [C]^T[B]^T D_l[B][C]dV = \frac{2\pi D_l}{\ln(r_0/r_c)} \int_L \begin{bmatrix} [N_e(s)]^T[N_e(s)] & -[N_e(s)]^T[N_c(s)] \\ -[N_c(s)]^T[N_e(s)] & [N_c(s)]^T[N_c(s)] \end{bmatrix} \frac{l}{2} ds \tag{3.31}$$

Now, we can combine contributions from all FE elements and dislocation segments to give the full set of equations and rewrite Eq. (3.14) as,

$$\begin{bmatrix} [K_E] & [K_{EC}] \\ [K_{EC}]^T & [K_C] \end{bmatrix} \begin{bmatrix} [\mu_e] \\ [\mu_c] \end{bmatrix} = \begin{bmatrix} [J_s] \\ [K_{vc}][v_l] \end{bmatrix} \tag{3.32}$$

where $[J_s]$ denotes the surface flux, which is zero for a closed system considered here. $[\mu_c]$ is the dislocation nodal chemical potential matrix, which can be derived from Eq. (2.18), and

$$[K_E] = \frac{2\pi D_l}{\ln(r_0/r_c)} \int_L [N_e(s)]^T[N_e(s)] \frac{l}{2} ds \tag{3.33}$$

$$[K_C] = \frac{2\pi D_l}{\ln(r_0/r_c)} \int_L [N_c(s)]^T[N_c(s)] \frac{l}{2} ds \tag{3.34}$$

$$[K_{EC}] = \frac{2\pi D_l}{\ln(r_0/r_c)} \int_L -[N_e(s)]^T[N_c(s)] \frac{l}{2} ds \tag{3.35}$$

Note that the value of r_0/r_c appears in the natural logarithm term, thus has a relatively subtle impact on the solution of the governing equation. As previously stated, they are parameters selected for the implementation of our methodology. In the present work, we used a value of $r_c = 2b$ based on previous work by Niu et al. (2019), and we set r_0 to 5 times r_c for our analysis, which is much less than the finite element size employed in all the simulations presented later.

We can then derive the chemical potential of the FE nodes $[\mu_e]$ and the lattice diffusion-controlled climb rate of dislocation nodes $[v_l]$:

$$[\mu_e] = [K_E]^{-1}\{[0] - [K_{EC}][\mu_c]\} \tag{3.36}$$

and

$$[v_l] = [K_{vc}]^{-1}\left([K_{EC}]^T[\mu_e] + [K_C][\mu_c]\right) \tag{3.37}$$

The above matrix equations represent a set of linear simultaneous equations which can be solved by any standard matrix method. The solution provides a climb rate of each individual dislocation node $[v_l]$, the nodal climb velocities can be derived as,

$$\boldsymbol{v}_l^I = v_l^I \boldsymbol{n}^I \tag{3.38}$$

where $\boldsymbol{n}^I$ is the weighted average of the slip plane normal of all segments connected to node I as defined in Liu et al. (2020b). Following the method used in the self climb model developed in our previous work Liu et al. (2020b), we can further incorporate the nodal climb velocity $\boldsymbol{v}_l^I$ into the three-dimensional DD framework to update the dislocation network caused by lattice diffusion-controlled climb.

4. Validation of the new model

Before moving on to the coupled lattice diffusion with core diffusion problem, a simple example of a lattice diffusion controlled climb process is first given, to compare with the available analytical solution to validate the procedures described above. The evolution of PDLs for various temperatures and loop sizes is then modeled, to illustrate the proposed method, to demonstrate that it produces accurate results by comparing with either available analytical results or physical observations, and to show how the simulations can be evaluated using the variational principle to provide simple macroscopic models of the way in which the microstructure evolves.

A simple example of lattice diffusion-controlled climb that can be solved analytically is the interaction of a pair of parallel edge dislocations in an infinite isotropic medium, as depicted in Fig. 3(a). The two edge dislocations, with the same Burgers vector **b**, are located at $X_1 = \{0, 0\}$ and $X_2 = \{x, y\}$, in the central area of the crystal, where the boundaries of the cores are denoted by Γ_1 and Γ_2, respectively. We consider the situation where no external stress is applied to the crystal and the Peach–Koehler force experienced by a dislocation arises from the stress field generated by the other dislocation, which depends on their relative locations. According to the Peach–Koehler formula, the interaction forces between two parallel edge dislocations can be determined readily (Anderson et al., 2017),

$$\mathbf{F}_{12} = -\mathbf{F}_{21} = \frac{Gb_1b_2}{2\pi(1-\nu)} \frac{x(x^2-y^2)}{(x^2+y^2)^2}\hat{\mathbf{x}} + \frac{Gb_1b_2}{2\pi(1-\nu)} \frac{y(3x^2+y^2)}{(x^2+y^2)^2}\hat{\mathbf{y}} \tag{4.1}$$

where $\mathbf{F}_{12}$ represents the force which dislocation 1 exerts on dislocation 2, and $\mathbf{F}_{21}$ represents the force exerted by dislocation 2 on dislocation 1. G is the shear modulus, b_1 and b_2 are the magnitudes of the Burgers vectors of dislocation 1 and 2, with $b_1 = b_2 = b$.

Table 1
Parameters of bcc Fe.

Parameters	Magnitude
Shear Modulus	$G = 83$ GPa
Poisson's ratio	$\nu = 0.29$
Burgers vector	$b = 2.473$ Å
migration energy	$U_m = 1.8034$ eV (Frost and Ashby, 1982)
Pre-exponential for lattice diffusion	$D^0_{lattice} = 1.18 \times 10^{-5}$ m^2/s (Frost and Ashby, 1982)
Pre-exponential for core diffusion	$D^0_c = a_c D^0_{core} = 1 \times 10^{-23}$ m^4/s (Frost and Ashby, 1982)

4.1. Analytic solution

Following Eq. (2.18), the chemical potential μ_c on the boundary of the dislocation core Γ can be derived from the climb force on the dislocation, so that,

$$\mu_{c2} = -\mu_{c1} = -\frac{\mathbf{F}_{12} \cdot \hat{\mathbf{y}}}{b} = -\frac{Gb}{2\pi(1-\nu)} \frac{y(3x^2+y^2)}{(x^2+y^2)^2} \tag{4.2}$$

The problem then reduces to a classical potential problem; when $y > 0$, the difference in chemical potential drives mass to flow from dislocation 1 to dislocation 2 by lattice diffusion, leading to the dislocations climbing in opposite directions. That is, dislocation 1 emits atoms and climbs upwards, while dislocation 2 absorbs atoms and climbs downwards. According to Eq. (2.12), the climb velocities resulting from the mass exchange between dislocations 1 and 2 are determined by the net volumetric flux across the boundary of the dislocation cores. For a radial diffusion pattern discussed here,

$$v_{l1} = -\frac{\oint_\Gamma j_l n_\Gamma d\Gamma}{b} = \frac{2\pi r}{b} D_l \frac{\partial \mu}{\partial r} = \frac{2\pi r D_l}{b} \frac{\mu_{c1} - \mu_r}{\ln(r/r_c)} \tag{4.3}$$

with μ_r denoting the chemical potential at position r. Consider $\mu_r = \mu_{c2}$ at $r = r_{12} = \sqrt{x^2+y^2}$, then

$$v_{l1} = \frac{2\pi D_l r_{12}}{b} \frac{\mu_{c1} - \mu_{c2}}{\ln(r_{12}/r_c)} = \frac{4\pi r_{12} D_l}{b^2} \frac{F_{12}}{\ln(r_{12}/r_c)} \tag{4.4}$$

$$v_{l2} = -v_{l1} \tag{4.5}$$

For iron, the activation energy for lattice diffusion is set as $E_{lattice} = E_{core}/0.6$ (Frost and Ashby, 1982), other parameters used here are listed in Table 1. We assume a radial distance between the two dislocations $r_{12} = 500b$, with $x = 300b$. $y = 400b$. So that the chemical potentials on the dislocation cores and the resulting climb velocities can be derived from the analytic solutions Eqs. (4.2) and (4.4),

$$\mu^1_c = -\mu^2_c = 5.1202 \times 10^7 \ \ \mathrm{N/m^2} \tag{4.6}$$

$$v_{l1} = -v_{l2} = 0.1611b \ \ \mathrm{m/s} \tag{4.7}$$

The chemical potential field of the dislocations in an infinite domain is demonstrated in Fig. 3(c).

4.2. Numerical solution

A practical way to model the parallel edge dislocation pair with infinite length in a three-dimensional DD framework within a finite domain is to set a pair of dislocation lines in a relatively large domain, to minimize the influence of the boundary with an acceptable cost of computation. Consider a pair of edge dislocations with the same length of $l = 3000b$ in the middle of a bcc iron box. As shown in 3 (b), the distance between dislocation lines is set as $r_{12} = 500b$, with a distance of $300b$ in the x direction and a distance of $400b$ in the y. The size of the simulation box is $1200b \times 1200b \times 3600b$. The parameters of iron used in the simulation are given in Table 1. We then calculate the chemical potential field and the resulting climb velocities based on the numerical climb model developed in Section 3. We limit our attention to the middle surface of the box to minimize the influence of the top and bottom surfaces. A typical meshed layer of the domain at the middle surface is shown in Fig. 3(b) with an element size of $120b$. This is much larger than the core radius r_c, of $2b$ used here , and much larger than the radius of the cylindrical region near the core $r_0 = 5r_c$ as well. The chemical potentials on the dislocation core at the middle surface of dislocations 1 and 2 are,

$$\mu^1_c = -\mu^2_c = 5.0612 \times 10^7 \ \ \mathrm{N/m^2} \tag{4.8}$$

In agreement with the analytical chemical potential calculated in Eq. (4.6). The full chemical potential field at the middle surface is demonstrated in Fig. 3(d). Note that the numerical chemical potential field is consistent with the analytical solution except at the region near the external boundary. This is due to the fact that Fig. 3(c) shows the analytical chemical potential field of an infinite domain, whereas Fig. 3(d) demonstrates the chemical potential field within a finite domain, with an additional boundary condition of the flux field, $\mathbf{j}_l \cdot \mathbf{n}_S = 0$ at the boundaries. As a result, the chemical potential gradient near the external boundaries is zero. This is illustrated in Fig. 3(d) as the equipotential lines are perpendicular to the boundaries, leading to the discrepancy in chemical

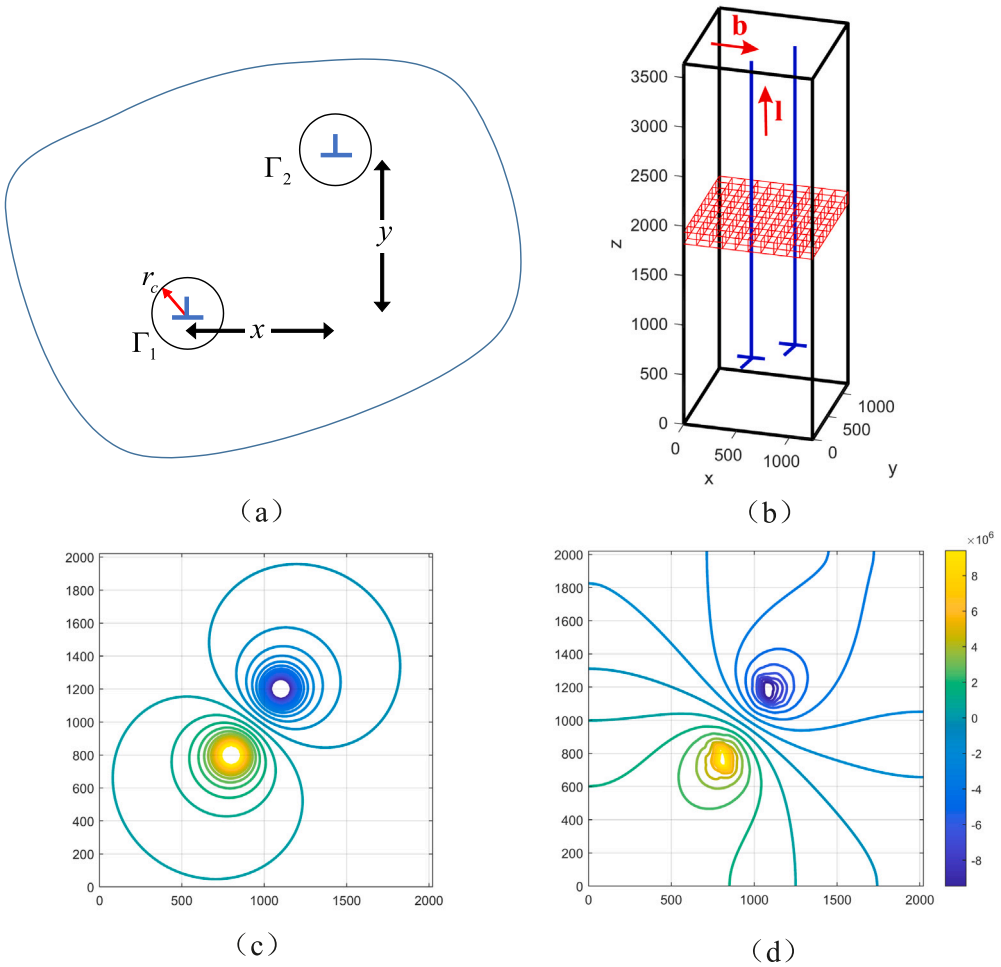

Fig. 3. (a) A two-dimensional view of a pair of parallel edge dislocations in an infinite domain, a distance of x and y apart from each other, (b) A pair of parallel edge dislocations in the finite domain, (c) Analytical solution of the chemical potential field, (d) Numerical result of the chemical potential field.

potential fields between the analytical and numerical results shown in Fig. 3(c) and (d). The resulting nodal climb velocities of the middle points of dislocations 1 and 2 can be calculated from Eq. (3.37),

$$v_l^1 = -v_l^2 = 0.1416b \ \text{m/s} \tag{4.9}$$

The differences between the numerical and analytical solutions for both chemical potential and climb velocity are plotted in Fig. 4 as a function of the size of the simulation box. The graph clearly shows that as the size of the simulation box increases, the difference between the numerical and analytical solutions decreases significantly. This can be attributed to the reduced influence of finite domain boundary conditions on the results, as the dislocation is farther away from the boundaries in a larger simulation box. There may be other possible errors in the analysis, as with any finite element approach. This relates to the accuracy of the chemical potential field that can be achieved with the chosen mesh and size of the near core element. There is also some duplication in contributions to the functional associated with the near core element (i.e. that due to the element itself and overlaying this is the contribution from the conventional finite element). However, if the near core region is much less than the element size any error introduced by not correcting should be negligible. This agreement between the numerical and analytical solutions for both chemical potential and climb velocity further confirms the validity of the newly developed lattice diffusion-controlled climb model; in contrast to the previous localization method (Liu et al., 2017b), by adopting the near core approximation, the present lattice diffusion model is independent of the FE elements size, as long as the size of the element satisfies the condition that $l_{element} \gg r_0, r_c$; therefore, it allows a much coarser finite element mesh to be employed, making it more efficient.

5. Application of the new model

A prismatic dislocation loop (PDL) is a disk-shaped layer of atoms/vacancies formed during thermal quenching (Silcox and Whelan, 1960), irradiation (Haley et al., 2019), or nanoindentation (Lee et al., 2020). Unlike a dislocation shear loop, the Burgers

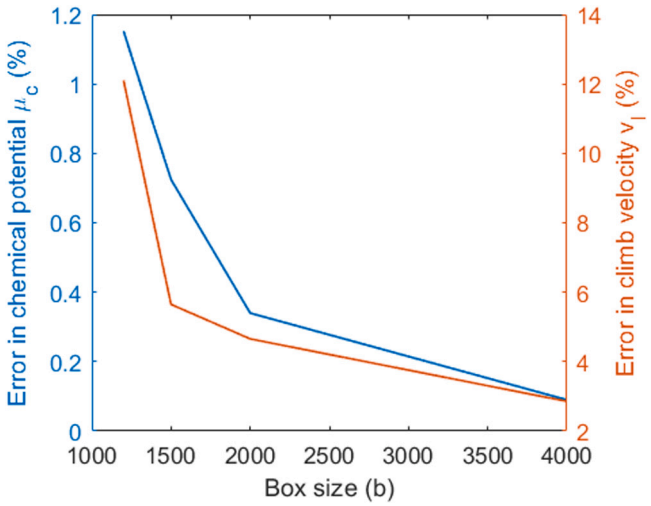

Fig. 4. Difference between the numerical and analytical solutions in the chemical potential and climb velocity as a function of the size of the simulation box.

vector of a PDL has a component normal to the habit plane. Therefore, the dislocation line can only glide on the glide cylinder of the loop, i.e. on the cylinder with its axis parallel to the Burgers vector. But loop translation can occur either by transferring atoms along the dislocation line by core diffusion or by exchanging atoms with the surrounding lattice by lattice diffusion, to move on its habit plane. Evolution of PDLs is widely used to study dislocation climb related processes (Kroupa, 1960; Mordehai et al., 2009; Niu et al., 2019; Liu et al., 2020b), because different types of dislocation motion, such as glide or self-climb, can be straightforwardly illustrated by the change of their sizes, positions, and loop profiles.

5.1. Coarsening of two PDLs

In this subsection, the evolution of two interstitial-type PDLs on the same habit plane is investigated. As shown in Fig. 5(a), the initial configuration is the two blue loops with initial radii of $R_1 = 12$ nm and $R_2 = 20$ nm, respectively. The distance between the centers of these two loops is $d = 42$ nm. They have the same Burgers vector pointing outward with a magnitude of $a/2\langle 111\rangle$, where a denotes the lattice parameter. In a bulk single crystal, without externally applied stress, the evolution of the PDLs will be driven by competition between the elastic interaction force and the line tension, to minimize the total energy and balance the forces. When loops lie in the same habit plane, the driving force in the glide direction, i.e. along the Burgers vector, is zero; this rules out the glide motion. In this case, the PDLs can only translate on their habit plane by climb.

We first focus our attention on lattice diffusion controlled climb. This allows a comparison with the coarsening model in the core diffusion controlled limit proposed by Liu et al. (2020b) and the experimental observation obtained by Swinburne et al. (2016), to validate the lattice diffusion model and to demonstrate the typical differences in the lattice and core diffusion processes. The simulated temperature was $T = 750$ K. Again, we adopted the relationship between the activation energy for lattice diffusion and that for core diffusion proposed by Frost and Ashby (1982), i.e. $E_{lattice} = E_{core}/0.6$. To compare with the results in Liu et al. (2020b), the same value of the activation energy, E_{core}, is adopted. With $D_{core} = D^0_{core}\exp(-\frac{E_{core}}{kT})$ and $D_{lattice} = D^0_{lattice}\exp(-\frac{E_{lattice}}{kT})$, an effective diffusivity for lattice diffusion $D_l = \frac{D_{lattice}\Omega}{kT} = 1.68\times10^{-34}$ m^{3}s^{-1}J^{-1} is derived from the effective core diffusivity D_c from Liu et al. (2020b). Other parameters for bcc iron used here are given in Table 1. Snapshots of the loop profile during the loop coarsening process by lattice diffusion are demonstrated in Fig. 5 (a)–(b), and the coarsening process by core diffusion, as reported by Liu et al. (2020b), is reproduced in Fig. 5(c)–(d) for comparison.

In the DD simulations, we assume that loops are far from surfaces and that there is no matter exchange at the external boundaries so dislocations are the only sources and sinks for atoms. The total number of atoms enclosed within the loops, i.e. the total enclosed loop area, should be constant during the evolution. The actual change of the total loop area during the simulation can therefore be taken as a measure of computing accuracy. In the lattice diffusion regime, the radii of the PDLs at the intermediate stage are $R_1' = 6.49$ nm, $R_2' = 22.56$ nm and the radius at the final stage is $R_l = 23.19$ nm, as shown in Fig. 5(a)–(b). So that $\pi R_1^2 + \pi R_2^2 \simeq \pi R_1'^2 + \pi R_2'^2 \simeq \pi R_l^2$, indicating the conservation of atoms. Similarly, in the core diffusion regime, the radius of the final single large loop is $R_c = 23.36$ nm and $\pi R_c^2 \simeq \pi R_1^2 + \pi R_2^2$. In each of the simulations examined above the total change in area was less than 1.3%.

Despite the fact that the two loops merge into one single large loop in both the lattice and core diffusion regimes, they differ from each other in (i) the time scales over which the coarsening occurs and (ii) the way the loops evolve. We next consider qualitatively the differences in turn.

First, consider the difference in time scales. Fig. 5(a)–(b) show the evolution of geometry for the two PDLs by lattice diffusion. There are approximately five orders of magnitude difference in time compared with that in the core diffusion process of Fig. 5(c)–(d);

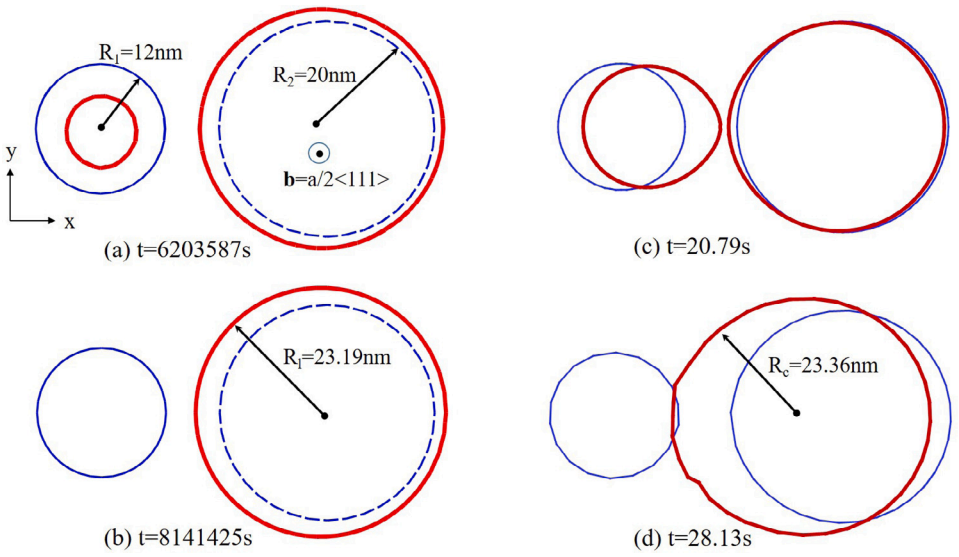

Fig. 5. Coarsening of two PDLs on the same habit plane. The thin blue line is the initial configuration, and the red line denotes the current loop profiles. (a)–(b) Snapshots of dislocation profiles during loop coarsening by lattice diffusion, (c)–(d) Snapshots of dislocation profiles during loop coarsening by core diffusion.

which is consistent with the theoretical prediction in Swinburne et al. (2016), confirming that at the experimental condition, i.e. at a low temperature of $T = 750$ K, coalescence of the two small PDLs is dominated by core diffusion.

Next, consider the difference in the way that loops evolve during the coalescence. In the lattice diffusion process, loop coalescence is achieved by two representative types of loop motion: (i) The large loop expands at the cost of the small loop via Oswald ripening; during this process, atoms are emitted from the smaller loop and deposit at the larger one, which is driven by the difference in line tensions between the loops — the smaller loop has a higher line tension, hence a higher climb force which leads to a higher chemical potential according to Eq. (2.18), so that atoms diffuse from the smaller loop to the larger one, resulting in the concentric expansion of the large loop and shrinkage of the small loop; this is consistent with experimental observations (Liu et al., 1995; Moll et al., 2013; Yuan et al., 2022). (ii) The two loops drift towards each other, as evidenced by the bias of the two sides of the final large loop relative to the original loop center, as shown in Fig. 5(b); in this process, the elastic interaction between loops results in a difference in the forces acting on the two sides of the same loop — segments close to the other loop experience larger elastic interaction forces compared to those that are far from the other loop, causing a difference in the climb force and, therefore, a difference in chemical potential on the two sides of each loop, according to Eq. (2.18). This leads to atoms diffusing out from one side of the loop and depositing at the other side, resulting in the drift of loops towards each other; which is not captured in existing models (Mordehai et al., 2009; Bakó et al., 2011; Liu et al., 2017a).

For a more straightforward illustration of these two different types of loop motion, we examine two extreme situations here: first consider the situation where the distance between loops, d, is very large, Fig. 6(a). As determined in Liu et al. (2020b), the elastic interaction force between loops is proportional to $1/d^4$, so that the elastic interaction force is negligible compared to the line tension; the evolution is then dominated by Oswald ripening. As shown in Fig. 6(a)–(d), the large loop expands concentrically by absorbing atoms diffusing from the smaller one. Next consider the situation where the two PDLs have the same radius, R, Fig. 6(e). In this case, the loops have the same line tension, elastic interaction between the loops causes the loops to drift towards each other and merge into one circular loop, as shown in Fig. 6 (e)–(h).

However, in core diffusion, atoms are transferred along the dislocation line, so that loops can only change their locations and shapes to drift towards each other before they intersect, as shown in Fig. 5(c); after which, the merged large loop evolves into a circular one by fast local atomic rearrangement, as shown in Fig. 5(d), to balance the chemical potential and minimize the total energy.

The above comparison between lattice and core diffusion mechanisms indicates that the evolution of loops by diffusion is temperature and length-scale dependent. This leads us to use parameters, such as temperatures or loop radius, as coordinates to construct a map in parameter space, in which each point represents a set of parameters. Boundaries exist to divide the space into regions over which each of the diffusion mechanisms is dominant. To do this, we discuss first the analytical solutions for the motion of an isolated PDL in the lattice and core diffusion regimes, respectively, to determine the controlling parameters.

5.2. A general diffusion mechanism map

It proves convenient to derive the analytical solution of loop motion by assuming the loop is rigid, i.e. it retains its shape and size during the evolution, so that only the rate of loop drift is considered here. We consider first the approximate solution for the motion of a circular PDL by lattice diffusion.

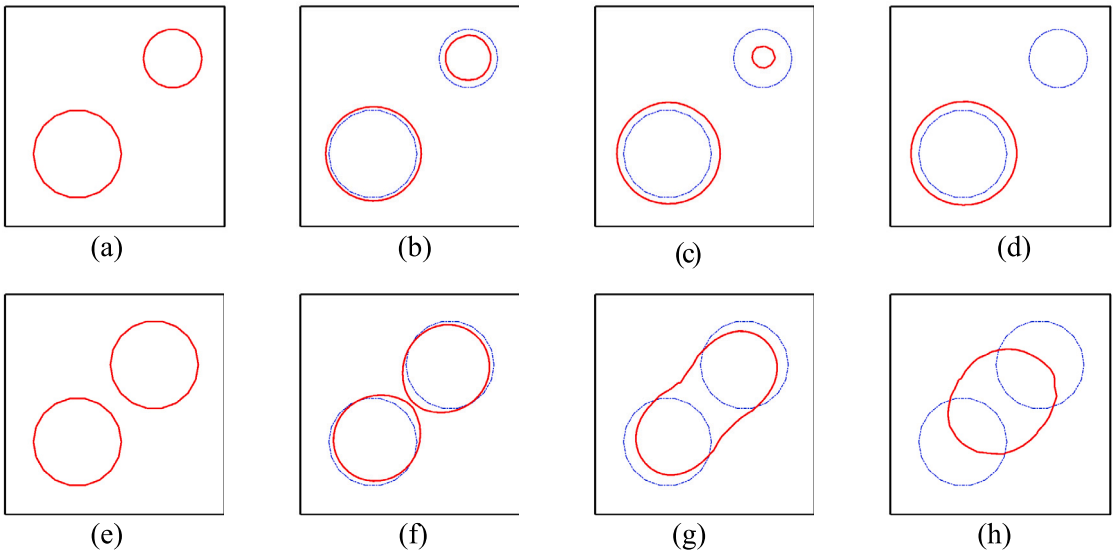

Fig. 6. Two extreme cases of the coarsening of two PDLs by lattice diffusion. (a)–(d) Loop coarsening via Oswald ripening; (e)–(h) Loop coarsening by drifting towards each other. Loops in blue represent the initial dislocation configuration and the current loop profiles are highlighted in red.

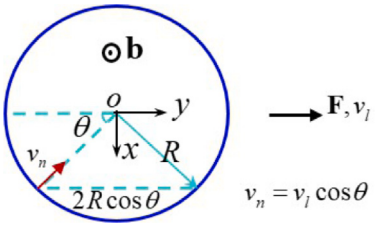

Fig. 7. Schematic illustration of the motion of a circular rigid PDL by lattice diffusion.

Consider the problem where a circular rigid PDL of radius R experiences a climb force F and moves at a velocity v_l under the action of this force, as schematically shown in Fig. 7. The climb rate for the center of the circular rigid PDL controlled by lattice diffusion can be approximately derived (see Appendix A for details) as,

$$v_l \approx \frac{D_l}{b^2}\frac{F}{R} \tag{5.1}$$

The climb rate of the same PDL by core diffusion has been derived by Liu et al. (2020b) as,

$$v_c = \frac{D_c}{\pi b^2}\frac{F}{R^3} \tag{5.2}$$

So that we have the climb rate ratio v_c/v_l,

$$\frac{v_c}{v_l} \approx \frac{D_c}{\pi R^2 D_l} \tag{5.3}$$

Note that,

$$D_c = \frac{a_c D_{core}\Omega}{kT} = \frac{a_c \Omega}{kT} D^0_{core} \exp\left(-\frac{E_{core}}{kT}\right) \tag{5.4}$$

$$D_l = \frac{D_{lattice}\Omega}{kT} = \frac{\Omega}{kT} D^0_{lattice} \exp\left(-\frac{E_{lattice}}{kT}\right) \tag{5.5}$$

So that,

$$\frac{v_c}{v_l} \approx \frac{D_{core} r_c^2}{D_{lattice} R^2} \tag{5.6}$$

where r_c is the dislocation core radius.

Now consider the climb rate ratio v_c/v_l. If the climb rate by lattice diffusion is negligible compared to that by core diffusion, $v_c/v_l \gg 1$, atoms mainly diffuse along the dislocation line. If the climb rate by lattice diffusion is appreciable, however, atoms can

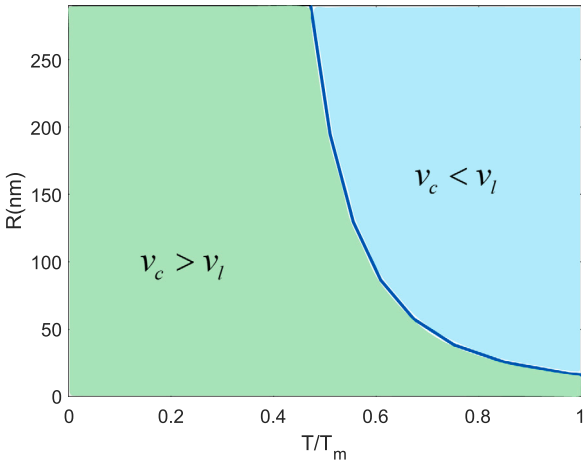

Fig. 8. The diffusion mechanism map. A boundary, where $v_c/v_l = 1$, separates the plane into two regions. A dislocation configuration with the parameter group falling under the boundary is dominated by core diffusion, and a dislocation configuration with parameters falling above the boundary is dominated by lattice diffusion.

also diffuse via the regular lattice. With the assumption that $E_{lattice} = E_{core}/0.6$, we can further construct a diffusion mechanism map. A point on the map represents a pair of parameters, loop radius R, with a unit of nm, and the homologous temperature, T, with a unit of T_m. T_m is the melting point of a given material which is 1811 K used here for iron. A boundary, where core diffusion and lattice diffusion contribute equally to the climb rate, i.e. $v_c/v_l = 1$, divides the plane into two regions. As shown in Fig. 8, in the region under the boundary, as highlighted in green, $v_c > v_l$, indicating that core diffusion is dominant. In the region above the boundary, as indicated in blue, when $v_c < v_l$, lattice diffusion dominates. It can be concluded from Fig. 8 that, the climb rate is dominated by core diffusion at low temperatures, particularly when the loop size is small; as the temperature increases, the contribution from lattice diffusion increases and eventually becomes dominant, which is more noticeable for larger loops. This agrees well with the numerical modeling from Breidi and Dudarev (2022). It is also worth noting that, for small loops, i.e. $R < 10$ nm, core diffusion plays a crucial role in their climb motion, even at elevated temperatures, which is of great importance for loop aggregation during post-irradiation annealing.

The diffusion mechanism map demonstrated above provides general guidelines for the dominant diffusion mechanism for a given set of parameters. As we have already demonstrated, the existence of the boundary and the relative locations of the regions in the diffusion mechanism map rely on general considerations. The details of the model only affect the exact position of the boundary. In most practical situations, lattice and core diffusion are competitive and synergistic at different stages of the loop evolution. It is, therefore, necessary to determine how loops evolve by a coupled core and lattice diffusion mechanism.

5.3. Loop coarsening by coupling lattice diffusion and core diffusion

In the above example, emphasis is put on the differences in the loop coarsening process by core and lattice diffusion, so that these regimes are considered separately. A natural question arises here — what will happen when we have a mixed mode of diffusion? In this section, we then examine situations, where the climb rate contributed from core and lattice diffusion are comparable, to demonstrate the competition and synergy between these two diffusion mechanisms.

Guided by Fig. 8, we design an example with carefully chosen temperature and loop sizes to illustrate the situation where core diffusion and lattice diffusion contribute comparable values to the climb rate to investigate the coupling effect. As shown in Fig. 9(a), three interstitial type PDLs with sizes of 20 nm, 60 nm and 100 nm lying on the same habit plane are set as the initial configuration. Note that the unit of length in the figures is the magnitude of the Burgers vector b. As discussed in the previous subsection, without externally applied stress, these PDLs will coalesce to minimize the total dislocation energy. The simulation temperature is chosen as $T = 0.7T_m$, at which the smallest loop will transfer by core diffusion to merge with the larger one, while the largest loop will expand by absorbing atoms through lattice diffusion, according to the diffusion mechanism map in Fig. 8.

Note that, although the diffusion mechanism map provides useful guidelines for the dominant diffusion mechanism for a given radius and temperature, it is not the full story. In addition to the loop size and temperature, another factor that influences the diffusion mechanism is the distance between the loops d – when loops are far from each other, elastic interaction forces between loops are negligible compare to line tension, Oswald ripening would be a more efficient way for matter exchange between loops. We then set the distances between the loops in the initial dislocation configuration, as shown in Fig. 9(a), to illustrate the contribution from core and lattice diffusion in a straightforward manner. Typical snapshots during the coalescence are shown in Fig. 9(a)–(f), where the red thick curve is the current dislocation configuration and the dashed blue line is the initial configuration. Two typical stages of loop evolution can be observed. During the first stage, as shown in Fig. 9(a)–(c), the smallest loop moves towards the larger one (in the middle) by changing its shape while maintaining its size before merging with the larger loop, Fig. 9(c); which is

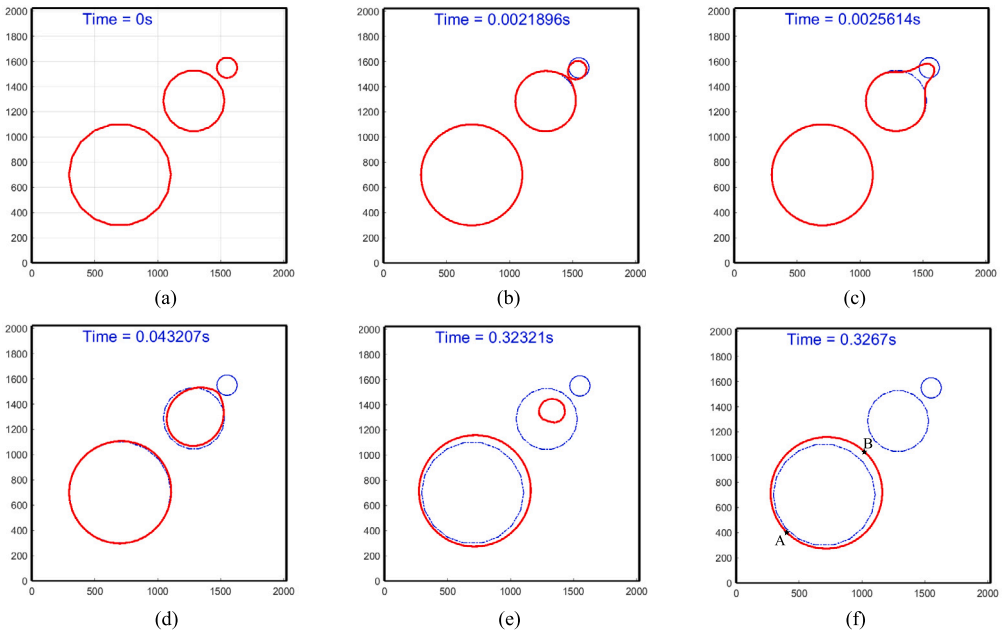

Fig. 9. Evolution of three PDLs with sizes of 20 nm, 60 nm and 100 nm. The unit of length in the figures is the magnitude of the Burgers vector $b = 0.2473$ nm.

similar to the coarsening process shown in Fig. 5(c)–(d), indicating that this process is dominated by core diffusion. It agrees well with the prediction from the diffusion mechanism map. During the second stage, as shown in Fig. 9(d)–(f), the larger loop expands at the expense of the smaller one without them being in contact with each other, and the coarsening rate is much slower compared to that of the first stage, demonstrating that this process is dominated by lattice diffusion. Note that, as the smaller loop shrinks, the parameter set of R and T moves downwards, in the diffusion mechanism map (Fig. 8), from the lattice diffusion dominant region to the core diffusion dominant region; the dominant mechanism, however, remains to be lattice diffusion because the distance between loops increases at the same time.

The evolution ends up with a single large loop with a radius of $R = 119.5$ nm, as shown in Fig. 9(f), which minimizes the total energy while conserving the total enclosed loop area. Meanwhile, a noticeable bias of the two sides of the final large loop from the original loop center, as shown by the location of point A and point B in Fig. 9(f), indicating that the drift of loops on the habit plane is driven by elastic interactions between loops via either core diffusion or lattice diffusion.

6. Conclusion

In the present paper, we have described a variational principle for the analysis of microstructure evolution in single crystalline materials. We demonstrated how a numerical scheme can be developed from it which naturally takes into account the competition and synergy between core diffusion and lattice diffusion. By incorporating the FE analysis into the nodal based three-dimensional DDD framework, the dislocation climb resulting from both core and lattice diffusion can be readily modeled, which allows the relative importance of different diffusion mechanisms to be identified and strategies to be developed so that the full range of possible situations can be systematically evaluated.

We limit our attention first to lattice diffusion, to validate the proposed numerical method by comparing it with the analytical solution of a typical simple example–the lattice diffusion controlled climb of a pair of parallel edge dislocations with infinite length. The numerical results agree well with the analytical solutions in both chemical potential on the dislocation cores and the resulting climb velocities. We then revisit the loop coarsening process of two PDLs sitting on the same habit plane, to compare with available experimental results (Swinburne et al., 2016) and numerical simulations (Liu et al., 2020b), to illustrate the characteristic loop profiles during the coarsening process controlled by core diffusion and lattice diffusion, respectively. Results indicate that at the experimental condition, i.e. at relatively low temperature, coalescence of small PDLs is dominated by core diffusion, and the resulting climb rate is five orders of magnitude higher than that for lattice diffusion. This is consistent with the theoretical predictions (Swinburne et al., 2016).

We have also shown how a diffusion mechanism map can be constructed using the approximate solutions for the motion of rigid circular PDLs by lattice and core diffusion. It provides a good indication of the dominant diffusion mechanism for any given loop size and temperature. Guided by this map, a loop coarsening process with carefully chosen temperature and loop sizes is further investigated based on the validated method, where contributions from lattice diffusion and core diffusion to the climb rate are comparable, to demonstrate the competition and synergy between these two diffusion mechanisms. Results demonstrate that, in a

practical loop coarsening process, core diffusion provides a fast short circuit for local atomic rearrangement, so that it dominates when loop size or the distance between loops is small, particularly at temperatures lower than $0.5T_m$. While, at high temperatures, when the distance between loops is large or when the loop size is large, lattice diffusion becomes more efficient. These findings provide guidance for the coalescence of PDLs, which is of significant importance for dislocation climb related mechanisms, such as creep and post-irradiation annealing.

In this paper, we have concentrated on modeling the dislocation climb process. The models considered here can readily be combined with models for glide and cross-slip, as described by Liu et al. (2021), to model the creep behavior of engineering materials.

Data accessibility

The code used for the discrete dislocation dynamic simulations is freely available from https://github.com/TarletonGroup/EasyDD.

CRediT authorship contribution statement

Fengxian Liu: Conceptualization, Methodology, Software, Formal analysis, Writing – original draft. **Alan C.F. Cocks:** Conceptualization, Methodology, Formal analysis, Writing – review & editing. **Edmund Tarleton:** Conceptualization, Software, Formal analysis, Writing – review & editing, Funding acquisition.

Declaration of competing interest

The authors declare that they have no known competing financial interests or personal relationships that could have appeared to influence the work reported in this paper.

Data availability

Data will be made available on request.

Acknowledgments

The authors are grateful to the Engineering and Physical Sciences Research Council (EPSRC), United Kingdom for funding through project grant EP/R013136/1. ET would like to thank the Royal Academy of Engineering, United Kingdom for support through a senior research Fellowship.

Appendix A. Approximate solution for the motion of a PDL by lattice diffusion

Consider the motion of a rigid circular PDL of radius R under the action of a climb force F, which moves at a velocity v_l under the action of this force, as schematically shown in Fig. 7. The lattice diffusion equation follows,

$$j_i = -D_l \frac{\partial \mu}{\partial x_i} = D_l f_i \tag{A.1}$$

where i has a value in the range of 1 to 3 and refers to a right-handed coordinate system. $f_i = -\frac{\partial \mu}{\partial x_i}$. The rate of energy dissipation per unit volume for material rearrangement due to lattice diffusion $\dot{d}$ can be expressed as $\dot{d} = j_i f_i$. So that the total energy dissipation rate is,

$$\dot{D} = \int_V j_i f_i dV = F v_l \tag{A.2}$$

This applies to the exact solution to the problem. The exact solution is that which minimizes the functional,

$$\Pi = \Psi + \dot{G} = \Psi - F v_l \tag{A.3}$$

where $\Psi = \int_V \frac{1}{2D_l} j_i j_i dV$. Note, v_l, j_i represent a suitable kinematic field, i.e., j_i is consistent with v_l.

If v_l', j_i' is the exact solution and v_l'', j_i'' is any arbitrary kinematic field, then,

$$\frac{1}{2D_l} \int_V j_i' j_i' dV - F v_l' \leq \frac{1}{2D_l} \int_V j_i'' j_i'' dV - F v_l'' \tag{A.4}$$

From Eqs. (A.1) and (A.2),

$$\frac{1}{2D_l} \int_V j_i' j_i' dV = \frac{1}{2} \int_V f_i' j_i' dV = \frac{1}{2} F V_L' \tag{A.5}$$

Substituting Eq. (A.5) into Eq. (A.4) gives,

$$\frac{1}{2} F v_l' \geq F v_l'' - \frac{1}{2D_l} \int_V j_i'' j_i'' dV \tag{A.6}$$

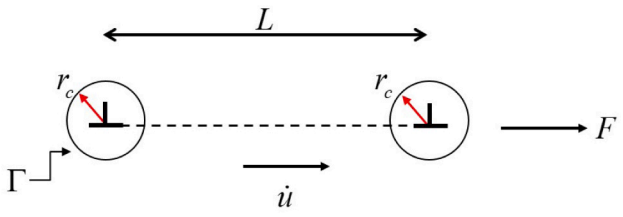

Fig. A.10. Schematic illustration of the motion of a pair of straight dislocations in 2D.

Now consider a mechanism such that

$$v_l'' = \lambda \hat{v}_l \tag{A.7}$$

$$j_l'' = \lambda \hat{j}_i \tag{A.8}$$

where $\hat{v}_l$ represents the form of the mechanism (shape function) and λ is the magnitude. Then Eq/(A.6) becomes

$$\frac{1}{2} F v_l' \geq \lambda F \hat{v}_l - \lambda^2 \frac{1}{2D_l} \int_V \hat{j}_l \hat{j}_l dV \tag{A.9}$$

Now choose the value of λ that maximizes the right-hand side of Eq. (A.9). Assume,

$$\Xi = \lambda F \hat{v}_l - \lambda^2 \frac{1}{2D_l} \int_V \hat{j}_l \hat{j}_l dV \tag{A.10}$$

for a prescribed $\hat{v}_l$, $\hat{j}_i$. The maximum value of Ξ appears when

$$\frac{d\Xi}{d\lambda} = F \hat{v}_l - \lambda \frac{1}{D_l} \int_V \hat{j}_l \hat{j}_l dV = 0 \tag{A.11}$$

So that,

$$\lambda = \frac{F \hat{v}_l}{\frac{1}{D_l} \int_V \hat{j}_l \hat{j}_l dV} \tag{A.12}$$

Substituting Eq. (A.12) into Eq. (A.9) gives,

$$\frac{1}{2} F v_l' \geq \frac{1}{2} \frac{(F \hat{v}_l)^2}{\frac{1}{D_l} \int_V \hat{j}_l \hat{j}_l dV} \tag{A.13}$$

i.e.,

$$v_l' = \frac{F \hat{v}_l^2}{\frac{1}{D_l} \int_V \hat{j}_l \hat{j}_l dV} \tag{A.14}$$

Note, (a) v_l' is proportional to the driving force F. (b) Both the numerator and the denominator of Eq. (A.14) are quadratic in the scale of the mechanism and therefore the result is independent of the scale of the mechanism that is chosen for the calculation. We can use Eq. (A.14) to obtain a bound to the velocity.

A.1. 2D problem

Now consider a 2D problem, as shown in Fig. A.10,

$$v_l = \frac{1}{b} \int_\Gamma j_r d\Gamma = \frac{1}{b} \oint j_r r_c d\theta \tag{A.15}$$

where the integral is around the dislocation core.

Assume a radial flux pattern, as shown in Fig. A.11, such that

$$\hat{j}_r = j_c r_c / r \tag{A.16}$$

where j_c is the radial flux at the core. Since the fan of the flow lines sweep through an angle of $2\theta_h$

$$\hat{v}_l = \frac{2 j_c r_c \theta_h}{b} \tag{A.17}$$

Now consider flux through a radial fan that subtends an angle $d\theta$. For this region,

$$\int_V \hat{j}_i \hat{j}_i dV = \int_\theta \int_{r_c}^{r} {j_c}^2 \frac{{r_c}^2}{r^2} r dr d\theta = \int_\theta {j_c}^2 {r_c}^2 \ln \frac{r}{r_c} d\theta \tag{A.18}$$

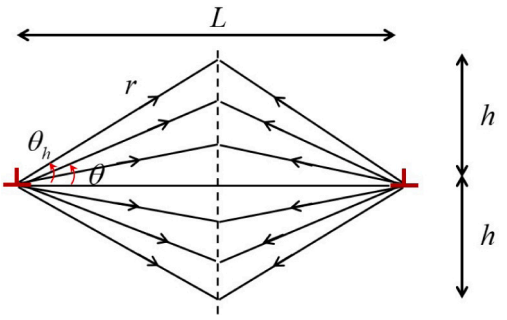

Fig. A.11. Schematic illustration of a radial flux pattern.

with $r = \frac{L}{2\cos\theta}$.

Summing all contributions gives

$$\int_V \hat{j}_i \hat{j}_i dV = 2\int_0^{\theta_h} {j_c}^2 {r_c}^2 \ln\frac{L}{2\cos\theta r_c} d\theta \tag{A.19}$$

$$= 2{j_c}^2 {r_c}^2 \left[\ln\frac{L}{2r_c}\theta_h - \int_0^{\theta_h} \ln(\cos\theta) d\theta\right] \tag{A.20}$$

$$= 2{j_c}^2 {r_c}^2 I(\frac{L}{r_c}, \theta_h) \tag{A.21}$$

where $I(\frac{L}{r_c}, \theta_h) = \ln\frac{L}{2r_c}\theta_h - \int_0^{\theta_h} \ln(\cos\theta) d\theta$ is a function of $\frac{L}{r_c}$ and θ_h.

Substituting Eqs. (A.17) and (A.21) into Eq. (A.14) gives,

$$v_l' = \frac{D_l F}{b^2} \frac{4j_c^2 r_c^2 \theta_h^2}{2j_c^2 r_c^2 I(\frac{L}{r_c}, \theta_h)} = \frac{2D_l F \theta_h^2}{b^2 I(\frac{L}{r_c}, \theta_h)} \tag{A.22}$$

Note, if θ_h is small,

$$v_l' = \frac{2D_l F \theta_h}{b^2 \ln\frac{L}{2r_c}} \tag{A.23}$$

Note also,

$$\frac{\theta_h^2}{I} = \frac{\theta_h}{\ln\frac{L}{2R_c} - \ln(\cos\theta_h) - \frac{1}{\theta_h}\int_0^{\theta_h} \theta tan\theta d\theta} \tag{A.24}$$

One might expect

$$v_l' = \kappa \frac{2D_l F \theta_h}{b^2 \ln\frac{L}{2r_c}} \tag{A.25}$$

where κ is a constant.

A.2. A circular loop

Now let us look at the circular loop shown in 7. Following the above description, the 2-D flow in plane is

$$v_n = v_l \cos\theta = \frac{2\pi F(\theta) D_l}{b^2 \ln\frac{2R\cos\theta}{r_c}} \tag{A.26}$$

where $F(\theta)$ is the force per unit length at θ. So that

$$F(\theta) = \frac{v_l b^2}{2\pi D_l} \cos\theta \ln\frac{2R\cos\theta}{r_c} \tag{A.27}$$

and

$$F = 4\int_0^R F(\theta) dx \tag{A.28}$$

$$= 4\int_0^{\pi/2} F(\theta) R\cos\theta d\theta \tag{A.29}$$

$$= \frac{2v_l b^2 R}{\pi D_l} \int_0^{\pi/2} \cos^2\theta \ln \frac{2R\cos\theta}{r_c} d\theta \tag{A.30}$$

$$= \frac{2v_l b^2 R}{\pi D_l} \left[\frac{\pi}{4} \ln \frac{2R}{r_c} + \int_0^{\pi/2} \cos^2\theta \ln\cos\theta d\theta \right] \tag{A.31}$$

i.e.,

$$F = \frac{v_l b^2 R}{2D_l} \left[\ln \frac{2R}{r_c} + \ln\alpha \right] \tag{A.32}$$

where $\ln\alpha = \frac{\pi}{4}\int_0^{\pi/2} \cos^2\theta \ln\cos\theta d\theta$. So that the climb velocity of a rigid circular PDL by lattice diffusion is,

$$v_l \approx \frac{2D_l}{b^2} \frac{F}{R \ln \frac{2R}{r_c}} \tag{A.33}$$

We can simplify this result further by noting that the result is not very sensitive to the ratio R/r_c. For the current purpose of determining the dominant mechanism over the range of conditions of interest here we can approximate Eq. (A.33) as

$$v_l \approx \frac{D_l F}{b^2 R} \tag{A.34}$$

References

Anderson, P.M., Hirth, J.P., Lothe, J., 2017. Theory of Dislocations. Cambridge University Press.

Ayas, C., Van Dommelen, J., Deshpande, V., 2014. Climb-enabled discrete dislocation plasticity. J. Mech. Phys. Solids 62, 113–136.

Bakó, B., Clouet, E., Dupuy, L.M., Blétry, M., 2011. Dislocation dynamics simulations with climb: kinetics of dislocation loop coarsening controlled by bulk diffusion. Phil. Mag. 91 (23), 3173–3191.

Breidi, A., Dudarev, S., 2022. Dislocation dynamics simulation of thermal annealing of a dislocation loop microstructure. J. Nucl. Mater. 562, 153552.

Cocks, A.C., 1989. A finite element description of grain-boundary diffusion processes in ceramic materials. Appl. Solid Mech. 3, 30–42.

Cocks, A., 1992. Interface reaction controlled creep. Mech. Mater. 13 (2), 165–174.

Cocks, A., 1996. Variational principles, numerical schemes and bounding theorems for deformation by Nabarro–Herring creep. J. Mech. Phys. Solids 44 (9), 1429–1452.

Cocks, A.C., Gill, S.P., Pan, J., 1998. Modeling microstructure evolution in engineering materials. In: Advances in Applied Mechanics, Vol. 36. Elsevier, pp. 81–162.

Davoudi, K.M., Nicola, L., Vlassak, J.J., 2012. Dislocation climb in two-dimensional discrete dislocation dynamics. J. Appl. Phys. 111 (10), 103522.

Frost, H.J., Ashby, M.F., 1982. Deformation Mechanism Maps: The Plasticity and Creep of Metals and Ceramics. Pergamon Press.

Gao, Y., Cocks, A., 2009. Thermodynamic variational approach for climb of an edge dislocation. Acta Mech. Solida Sin. 22 (5), 426–435.

Garbrecht, M., Saha, B., Schroeder, J.L., Hultman, L., Sands, T.D., 2017. Dislocation-pipe diffusion in nitride superlattices observed in direct atomic resolution. Sci. Rep. 7 (1), 1–7.

Geslin, P.A., Appolaire, B., Finel, A., 2015. Multiscale theory of dislocation climb. Phys. Rev. Lett. 115 (26), 265501.

Gill, S., Cocks, A., 1996. A variational approach to two dimensional grain growth—II. Numerical results. Acta Mater. 44 (12), 4777–4789.

Gu, Y., Xiang, Y., Quek, S.S., Srolovitz, D.J., 2015. Three-dimensional formulation of dislocation climb. J. Mech. Phys. Solids 83, 319–337.

Gu, Y., Xiang, Y., Srolovitz, D.J., El-Awady, J.A., 2018. Self-healing of low angle grain boundaries by vacancy diffusion and dislocation climb. Scr. Mater. 155, 155–159.

Haley, J., Liu, F., Tarleton, E., Cocks, A., Odette, G., Lozano-Perez, S., Roberts, S., 2019. Helical dislocations: Observation of vacancy defect bias of screw dislocations in neutron irradiated Fe–9Cr. Acta Mater. 181, 173–184.

Keralavarma, S., Benzerga, A., 2015. High-temperature discrete dislocation plasticity. J. Mech. Phys. Solids 82, 1–22.

Kroupa, F., 1960. Circular edge dislocation loop. Cechoslov. Fiziceskij Zurnal B 10 (4), 284–293.

Lee, S., Vaid, A., Im, J., Kim, B., Prakash, A., Guénolé, J., Kiener, D., Bitzek, E., Oh, S.H., 2020. In-situ observation of the initiation of plasticity by nucleation of prismatic dislocation loops. Nature Commun. 11 (1), 1–11.

Legros, M., Dehm, G., Arzt, E., Balk, T.J., 2008. Observation of giant diffusivity along dislocation cores. Science 319 (5870), 1646–1649.

Liu, F., Cocks, A.C., Gill, S.P., Tarleton, E., 2020a. An improved method to model dislocation self-climb. Modelling Simul. Mater. Sci. Eng. 28 (5), 055012.

Liu, F., Cocks, A.C., Tarleton, E., 2020b. A new method to model dislocation self-climb dominated by core diffusion. J. Mech. Phys. Solids 135, 103783.

Liu, F., Cocks, A.F., Tarleton, E., 2021. Dislocation dynamics modelling of the creep behaviour of particle-strengthened materials. Proc. R. Soc. Lond. Ser. A Math. Phys. Eng. Sci. 477 (2250), 20210083.

Liu, J., Law, M., Jones, K., 1995. Evolution of dislocation loops in silicon in an inert ambient—I. Solid-State Electron. 38 (7), 1305–1312.

Liu, F., Liu, Z.-l., Lin, P., Zhuang, Z., 2017a. Numerical investigations of helical dislocations based on coupled glide-climb model. Int. J. Plast. 92, 2–18.

Liu, F., Liu, Z., Pei, X., Hu, J., Zhuang, Z., 2017b. Modeling high temperature anneal hardening in Au submicron pillar by developing coupled dislocation glide-climb model. Int. J. Plast. 99, 102–119.

Love, G., 1964. Dislocation pipe diffusion. Acta Metall. 12 (6), 731–737. http://dx.doi.org/10.1016/0001-6160(64)90220-2, URL: https://www.sciencedirect.com/science/article/pii/0001616064902202.

Moll, S., Jourdan, T., Lefaix-Jeuland, H., 2013. Direct observation of interstitial dislocation loop coarsening in α-iron. Phys. Rev. Lett. 111 (1), 015503.

Mordehai, D., Clouet, E., Fivel, M., Verdier, M., 2008. Introducing dislocation climb by bulk diffusion in discrete dislocation dynamics. Phil. Mag. 88 (6), 899–925.

Mordehai, D., Clouet, E., Fivel, M., Verdier, M., 2009. Annealing of dislocation loops in dislocation dynamics simulations. In: IOP Conference Series: Materials Science and Engineering, Vol. 3. IOP Publishing, 012001.

Needleman, A., Rice, J., 1983. Plastic creep flow effects in the diffusive cavitation of grain boundaries. In: Perspectives in Creep Fracture. Elsevier, pp. 107–124.

Nicolas, J., Assali, S., Mukherjee, S., Lotnyk, A., Moutanabbir, O., 2020. Dislocation pipe diffusion and solute segregation during the growth of metastable gesn. Cryst. Growth Des. 20 (5), 3493–3498.

Niu, X., Gu, Y., Xiang, Y., 2019. Dislocation dynamics formulation for self-climb of dislocation loops by vacancy pipe diffusion. arXiv preprint arXiv:1901.05174.

Niu, X., Luo, T., Lu, J., Xiang, Y., 2017. Dislocation climb models from atomistic scheme to dislocation dynamics. J. Mech. Phys. Solids 99, 242–258.

Pan, J., Cocks, A., 1995. A numerical technique for the analysis of coupled surface and grain-boundary diffusion. Acta Metall. Mater. 43 (4), 1395–1406.

Pan, J., Cocks, A., Kucherenko, S., 1997. Finite element formulation of coupled grain-boundary and surface diffusion with grain-boundary migration. Proc. R. Soc. Lond. Ser. A Math. Phys. Eng. Sci. 453, 2161–2184.

Po, G., Ghoniem, N., 2014. A variational formulation of constrained dislocation dynamics coupled with heat and vacancy diffusion. J. Mech. Phys. Solids 66, 103–116.
Schwink, C., Nortmann, A., 1997. The present experimental knowledge of dynamic strain ageing in binary fcc solid solutions. Mater. Sci. Eng. A 234, 1–7.
Shewmon, P., 2016. Diffusion in Solids. Springer.
Silcox, J., Whelan, M., 1960. Direct observations of the annealing of prismatic dislocation loops and of climb of dislocations in quenched aluminium. Phil. Mag. 5 (49), 1–23.
Suo, Z., 1997. Motions of microscopic surfaces. Adv. Appl. Mech. 33, 193–294.
Swinburne, T.D., Arakawa, K., Mori, H., Yasuda, H., Isshiki, M., Mimura, K., Uchikoshi, M., Dudarev, S.L., 2016. Fast, vacancy-free climb of prismatic dislocation loops in bcc metals. Sci. Rep. 6, 30596.
Van der Giessen, E., Needleman, A., 1995. Discrete dislocation plasticity: a simple planar model. Modelling Simul. Mater. Sci. Eng. 3 (5), 689.
Vengrenovich, R., Gudyma, Y., Yarema, S., 2002. Ostwald ripening under dislocation diffusion. Scr. Mater. 46 (5), 363–367. http://dx.doi.org/10.1016/S1359-6462(01)01252-0, URL: https://www.sciencedirect.com/science/article/pii/S1359646201012520.
Yuan, Q., Chauhan, A., Gaganidze, E., Aktaa, J., 2022. Dislocation loop coarsening and shape evolution upon annealing neutron-irradiated RAFM steel. J. Nucl. Mater. 558, 153366. http://dx.doi.org/10.1016/j.jnucmat.2021.153366, URL: https://www.sciencedirect.com/science/article/pii/S0022311521005791.